Separating polarization components through the electro-optic read-out of photorefractive solitons

A. Pierangelo[1,2], E. DelRe[1,3*], A. Ciattoni[4], G. Biagi[1], E. Palange[1,4], A. Agranat[5]

[1]*Laboratorio di Ottica e Fotonica, Dipartimento di Ingegneria Elettrica e dell'Informazione, Università dell'Aquila, Monteluco di Roio 67100 L'Aquila, Italy*
[2]*Dipartimento di Fisica, Università di Roma "La Sapienza", 00185 Rome, Italy*
[3]*CRS SOFT, INFM-CNR, Università di Roma "La Sapienza", 00185 Roma, Italy*
[4]*Consiglio Nazionale delle Ricerche - CASTI Regional Lab, 67100 L'Aquila, Italy*
[5]*Department of Applied Physics, Hebrew University of Jerusalem, Jerusalem 91904, Israel*

*edelre@ing.univaq.it

Abstract: Analyzing the propagation dynamics of a light beam of arbitrary linear input polarization in an electro-activated photorefractive soliton we are able to experimentally find the conditions that separate its linear polarization components, mapping them into spatially distinct regions at the crystal output. Extending experiments to the switching scheme based on two oppositely biased solitons, we are able to transform this spatial separation into a separation of two distinct guided modes. The result is a miniaturized electro-optic polarization separator.

© 2007 Optical Society of America

OCIS codes: (160.2100) Electro-optical materials; (190.5330) Photorefractive nonlinear optics; (230.5440) Polarization-sensitive devices.

References and links

1. M. Segev, B. Crosignani, A. Yariv, and B. Fischer, "Spatial solitons in photorefractive media," Phys. Rev. Lett. **68**, 923–926 (1992).
2. M. Morin, G. Duree, G. Salamo, and M. Segev, "Wave-guides formed by quasi-steady-state photorefractive spatial solitons," Opt. Lett. **20**, 2066-2068 (1995).
3. M.F. Shih, M. Segev, and G. Salamo, "Circular waveguides induced by two-dimensional bright steady-state photorefractive spatial screening solitons," Opt. Lett. **21**, 931-933 (1996).
4. E. DelRe, M. Tamburrini, M. Segev, E. Refaeli, A.J. Agranat, "Two-dimensional photorefractive spatial solitons in centrosymmetric paraelectric potassium-lithium-tantalate-niobate," Appl. Phys. Lett. **73**, 16-18 (1998).
5. M. Chauvet, A.Q. Gou, G.Y. Fu, G. Salamo, "Electrically switched photoinduced waveguide in unpoled strontium barium niobate," J. Appl. Phys. **99**, 113107 (2006).
6. M. Asaro, M. Sheldon, Z.G. Chen, O. Ostroverkhova, W.E. Moerner, "Soliton-induced waveguides in an organic photorefractive glass," Opt. Lett. **30**, 519-521 (2005).
7. E. DelRe, M. Tamburrini, A.J. Agranat, "Soliton electro-optic effects in paraelectrics," Opt.Lett. **25**, 963-965 (2000).
8. E. DelRe, B. Crosignani, P. Di Porto, E. Palange, A.J. Agranat, "Electro-optic beam manipulation through photorefractive needles," Opt. Lett. **27**, 2188-2190 (2002).
9. A. Bitman, N. Sapiens, L. Secundo, A.J. Agranat, G. Bartal, M. Segev, "Electroholographic tunable volume grating in the (g44) configuration," Opt. Lett. **31**, 2849-2851 (2006).
10. M. Segev, G. C. Valley, S.R. Singh, M.I. Carvalho, and D.N. Christodoulides, "Vector photorefractive spatial solitons," Opt. Lett. **20**, 1764-1766 (1995).
11. C. Crognale and L. Rosa, "Vector analysis of the space-charge field in nonconventionally biased photorefractive crystals ," J. Lightwave Technol. **23**, 2175-2185 (2005).

12. P. Zhang, J. Zhao, C. Lou, X. Tan, Y. Gao, Q. Liu, D. Yang, J. Xu, and Z. Chen, "Elliptical solitons in nonconventionally biased photorefractive crystals," Opt. Exp. **15**, 536-544 (2007).
13. A. Agranat, R. Hofmeister, A. Yariv, Opt. Lett. **17**, 713-715 (1992)
14. A. Yariv and P. Yeh, *Optical Waves in Crystals* (Wiley, New York, 2002).
15. A.A. Zozulya and D.Z. Anderson, "Propagation of an optical beam in a photorefractive medium in the presence of a photogalvanic nonlinearity or an externally applied electric-field," Phys. Rev. A **51**, 1520-1531 (1995).
16. E. DelRe, A. Ciattoni, A.J. Agranat, "Anisotropic charge displacement supporting isolated photorefractive optical needles ," Opt. Lett. **26**, 908-910 (2001).
17. A. Zozulya and D. Anderson, "Nonstationary self-focusing in photorefractive media," Opt. Lett. **20**, 837-839 (1995).
18. C. Dari-Salisburgo, E. DelRe, E. Palange, "Molding and stretched evolution of optical solitons in cumulative nonlinearities," Phys. Rev. Lett. **91**, 263903 (2003).
19. S. Gatz, J. Herrmann, "Anisotropy, nonlocality, and space-charge field displacement in (2+1)-dimensional self-trapping in biased photorefractive crystals," Opt. Lett. **23**, 1176-1178 (1998).
20. E. DelRe, A. D'Ercole, E. Palange, A.J. Agranat, "Observation of soliton ridge states for the self-imprinting of fiber-slab couplers," Appl. Phys. Lett. **86**, 191110 (2005).

1. Introduction and motivation

Photorefractive solitons can be used to write semi-permanent volume space-charge patterns that passively guide and steer longer wavelength or less intense beams [1, 2, 3]. The procedure is a typical two-step read-write scheme: a nonlinear beam forms the soliton in conditions in which absorption occurs (write), and either simultaneously or when the write beam has been turned-off a non-absorbed beam is linearly guided through the previously imprinted pattern (read). An important issue is how this pattern can be changed and rearranged. In crystals that have a linear electro-optic effect the pattern can be altered only through a successive writing phase, involving slow charge-separation and absorption, and the pattern can hence be considered functionally static. In crystals with a quadratic electro-optic effect, such as paraelectrics, unpoled ferroelectrics, and disordered glasses [4, 5, 6], the nonlinear combination of the soliton space-charge with the applied external bias allows a purely electro-optic manipulation on command without the requirement of further charge separation or rearrangement. The external electric control field is thus capable of rapidly rendering guiding or antiguiding a given soliton pattern (soliton electro-activated pattern) [7, 8]. Both the static and electro-activated patterns form through birefringence, and this makes them intrinsically polarization sensitive. Conventional schemes aimed at guiding and steering reduce and simplify the system to an approximately scalar propagation by having both the soliton and the passively guided beam linearly polarized along the natural or induced optical axis, and hence the birefringence does not appreciably affect the polarization. From the purely nonlinear perspective, i.e., in the writing phase, effects resulting from the interaction of different polarization states have been predicted in Ref.[10], whereas a recent effort has been dedicated to the study of effects of unconventional bias field directions [11, 12], a geometry that can equally activate polarization change.

In this paper our focus is on how an imprinted soliton pattern can be used on read-out to electro-optically manipulate polarization, an extension of functionality that parallels that recently begun for electro-holography, where the use of a spatially resolved index of refraction ellipsoid allows electrically tunable wavelength filters [9]. We investigate light behavior in the read-out of an electro-activated soliton pattern when the light beam enters with an arbitrary linear input polarization. We are able to identify a specific geometry that allows the separation of input polarization components, providing a first demonstration of a soliton-based polarization analyzer.

#84618 - $15.00 USD Received 28 Jun 2007; revised 31 Aug 2007; accepted 2 Sep 2007; published 12 Oct 2007
(C) 2007 OSA

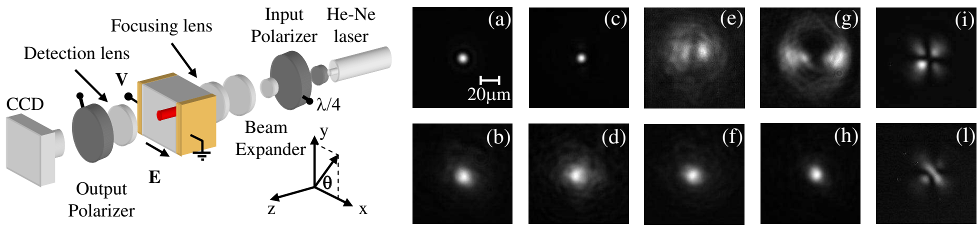

Fig. 1. Left: Experimental setup. Right: Propagation dynamics in the readout of an electro-activated soliton pattern. (a) input and (b) output intensity distribution before charge separation and (c)-(l) output for various conditions of θ_{in}, θ_{out}, and bias V.

2. Experiment

The experimental set-up is illustrated in Fig.(1). A $\lambda/4$ waveplate followed by a polarizer acting on the polarized laser beam is used to generate a read-out beam of arbitrary linear polarization, at an angle θ_{in} with respect to the x direction. An output polarizer selects the linear polarization at the angle θ_{out}. The photorefractive crystal was a zero-cut $L_x = 3$mm, $L_y = 2.4$mm, $L_z = 1$mm sample of potassium-lithium-tantalate-niobate (KLTN) doped with Copper and Vanadium impurities [13]. The crystal has a ferroelectric phase-transition at $T_c \simeq 14°$C. The temperature is fixed to $T \simeq 19°$C in the paraelectric phase, where the electro-optic response is quadratic and the dielectric constant is $\varepsilon_r \simeq 1.9 \times 10^4$. The quadratic electro-optic tensor reflects the m3m symmetry [14], with the coefficients $g_{11} \simeq 0.16\,\mathrm{m^4C^{-2}}$, $g_{12} \simeq -0.02\,\mathrm{m^4C^{-2}}$, and $g_{44} \simeq 0.08\,\mathrm{m^4C^{-2}}$, and a background index of refraction $n_0 \simeq 2.35$. The crystal is biased along the x-direction by applying a voltage V to planar electrodes on the opposite x-facets. The transmitted beam intensity distribution is imaged through a CCD camera. The soliton is generated as a quasi-steady-state two-dimensional self-trapped beam [1, 2, 3] by launching a continuous-wave $\lambda = 633\,$nm Gaussian beam from a He-Ne laser along the z-direction, with $\theta_{in} = 0$, i.e. polarized along the x-direction parallel to the bias electric field, and focusing it onto the input x,y facet of the crystal. The input beam Full-Width-at-Half-Maximum (FWHM) was $\Delta x \simeq \Delta y \simeq 8\,\mu$m (Fig.(1)a). For $V = 0$ the beam spreads due to linear diffraction to $\Delta x \simeq \Delta y \simeq 15\,\mu$m at output (Fig.(1)b, for $\theta_{out} = \theta_{in}$). Applying $V = V_{sol} \simeq -1.2\,$kV the beam traps into a soliton with output $\Delta x \simeq 7\,\mu$m and $\Delta y \simeq 8\,\mu$m after an interval $\tau_w \simeq 60\,s$ for an input power of $5\,\mu$W (Fig.(1)c, and again $\theta_{out} = \theta_{in}$). At this point, the soliton forming beam is blocked and the space-charge pattern remains locked into the acceptor impurities of the sample.

3. Results

Readout propagation is analyzed by launching the identical beam used to generate the soliton, but with a strongly attenuated power of 100 nW. In this case the space-charge remains unaltered for the whole duration of our experiments which is much less than the characteristic pattern decay time $\tau_r \simeq 50\tau_w$. The process amounts to a passive linear propagation dependent on the values of the applied electro-activation voltage V (in general different from V_{sol}). In an actual device, this guiding and manipulation would ideally be carried out on a longer wavelength, for example at $\lambda \simeq 1.5\,\mu$m, for which photorefractive absorption is ineffective [13].
In particular, we analyzed the three principal conditions of electro-activation: $V_+ = V_{sol}$, $V_0 = 0$, $V_- = -V_{sol}$ [8]. These three configurations correspond, in the standard scalar readout case

#84618 - $15.00 USD Received 28 Jun 2007; revised 31 Aug 2007; accepted 2 Sep 2007; published 12 Oct 2007
(C) 2007 OSA

where polarization is always kept parallel to the direction of the applied bias field, respectively to rendering guiding the patterns associated to the solitons formed with a writing bias $V = V_{sol}$ and rendering antiguiding those formed at $V = -V_{sol}$ (V_+ case); rendering antiguiding all soliton patterns (V_0 case); and rendering antiguiding the solitons formed with V_{sol} and guiding the ones formed with $-V_{sol}$ (V_- case). The strongly modified picture of single-soliton electro-activated readout for different input polarization states is shown in Fig.(1). For $V = V_+$, $\theta_{in} = 0$, the output beam component $\theta_{out} = 0$ is guided and obviously identical to the soliton case of Fig.(1c). For $\theta_{in} = \theta_{out} = \pi/2$, the beam diffracts to approximately 17 μm (Fig.(1)d), slightly more than the case of Fig.(1b). Next, for V_0 and $\theta_{in} = \theta_{out} = 0$ we detected the well-know two-lobe structure [15, 16], the central waveguide manifesting an antiguiding effect (Fig.(1e)). For $\theta_{in} = \theta_{out} = \pi/2$, the beam spreads to $\simeq 14\,\mu$m (Fig.(1f)). The last case of V_-, for $\theta_{in} = \theta_{out} = 0$ the waveguide is strongly antiguiding (Fig.(1)g). For $\theta_{in} = \theta_{out} = \pi/2$, the beam is weakly guided in the center of the pattern with an output $\Delta x \simeq 11\,\mu$m and $\Delta y \simeq 13\,\mu$m (Fig.(1h)).

We finally analyzed transmission in all previous cases for $\theta_{in} = 0, \pi/2$ and $\theta_{out} = \pi/2, 0$ (crossed polarizers), observing only a weak output intensity distribution. Increasing the exposure of the CCD camera by a factor of $\simeq 80$, we were able to detect the output distribution. For example, for the case of V_0, for $\theta_{in} = 0$ $\theta_{out} = \pi/2$ we observe the quadrifoil-like pattern of Fig.(1i), and for $\theta_{in} = \pi/2$ and $\theta_{out} = 0$ the pattern of Fig.(1l). This means that for the conditions analyzed, both the soliton and the waveguiding process is to a good approximation scalar, i.e., the polarization does not change. The weak cross-polarizer patterns are associated to the tensorial nature of the electro-optic response, in turn associated with the off-diagonal terms g_{44} [14].

4. Polarization separation

For a soliton written with V_{sol}, readout with an opposite bias $V_- = -V_{sol}$ allows the separation of the polarization components at output (see Fig.(1g,h)). The reason behind this effect is made evident analyzing the underlying index pattern distribution in the various cases, as discussed in the next Section. In general, the process can be described by the slowly-varying envelope of the input optical field $\mathbf{A}(x,y,z=0) = A(x,y,0)(\cos\theta_{in}\hat{\mathbf{e}}_x + \sin\theta_{in}\hat{\mathbf{e}}_y)$ that evolves to a general output field $\mathbf{A}(x,y,z=L_z) = [B_{xx}(x,y)\cos\theta_{in} + B_{xy}(x,y)\sin\theta_{in}]\hat{\mathbf{e}}_x + [B_{yx}(x,y)\cos\theta_{in} + B_{yy}(x,y)\sin\theta_{in}]\hat{\mathbf{e}}_y$ where $B_{ij}(x,y)$ is the output shape of the $i-$ cartesian field components due to the input $j-$ cartesian field component. B_{xy} and B_{yx} are responsible for the energy redistribution from input to output, associated with off-diagonal terms in the electro-optic tensor. Since we observed (see Fig(2)) that the output energy distribution follows the law $W_x = \int dxdy|A_x(x,y,L_z)|^2 = W_{tot}\cos^2\theta_{in}$ and $W_y = \int dxdy|A_y(x,y,L_z)|^2 = W_{tot}\sin^2\theta_{in}$, where $W_{tot} = W_x + W_y$, this implies that B_{xy} and B_{yx} are negligible with respect to B_{xx} and B_{yy}. Thus the separation does not involve an energy redistribution, so that for V_- the pattern truly acts as a separator of input polarization components.

The next step is to have both the separated components propagate in a guided fashion. This is achieved using a two-soliton pattern. The first soliton S_1 is formed with the writing bias $V_{S_1} = V_{sol} = -1.2$kV (Fig.(3)a). The second soliton S_2 is formed parallel to S_1 but shifted along the x-direction of 15 μm, with an opposite bias $V_{S_2} = -V_{S_1}$ (Fig.(3)c), using a technique described in detail in Ref.[8]. S_1 and S_2 are formed in sequence. Even though laterally shifted, the writing of S_2 is normally impaired by the fact that for V_{S_2} the pattern of S_1 becomes strongly antiguiding. However, this antiguiding has a negligible effect if S_2 is formed exactly where the space-charge pattern underlying S_1 has a lateral lobe [15], because in distinction to all other regions, here its response is actually weakly guiding for an opposite read-out bias [16] (Fig.(3b)).

The input read-out beam of arbitrary polarization, whose components at $\theta_{in} = 0$ and $\theta_{in} =$

#84618 - $15.00 USD Received 28 Jun 2007; revised 31 Aug 2007; accepted 2 Sep 2007; published 12 Oct 2007
(C) 2007 OSA

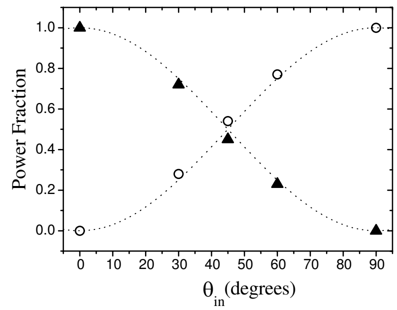

Fig. 2. Observed fraction of output power of the separated polarization components along x (triangles) and y (circles) and input for various values of θ_{in} and $V = -V_{sol}$. The dotted line is the case in which the relative power distribution is preserved from input to output.

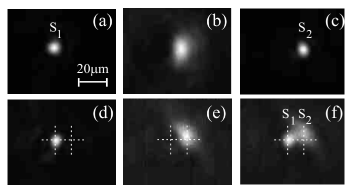

Fig. 3. A two-soliton polarization component separator. (a) S_1 soliton output at $V_{S_1} = V_{sol}$ after τ_w; (b) Output before the S_2 writing phase at $V = -V_{sol}$, having shifted the beam laterally by 15 μm; (c) S_2 output at $V_{S_2} = -V_{sol}$ after a second interval τ_w; read-out phase at $V = V_{sol}$, launching light into the S_2 core with $\theta_{in} = \pi/4$, (d) with $\theta_{out} = 0$, (e) $\theta_{out} = \pi/2$, and (f) no output polarizer. Crosses provide the reference to the two underlying soliton positions.

$\pi/2$ we wish to separate and guide, is launched where S_2 has been written, and a readout $V_+ = V_{S_1}$ is applied. The two components $\theta_{in} = 0$ and $\theta_{in} = \pi/2$ are separated and approximately guided in the patterns of S_1 and S_2 respectively, as shown in Fig.(3d-f) (for the case $\theta_{in} = \pi/4$). Again the separation of the input components is confirmed by a transmission analysis analogous to Fig.(2). The mechanism can once again be understood analyzing the underlying index patterns, as described in the next Section.

5. Numerical results and physical mechanism

The physical mechanism underlying the effect can be grasped by analyzing theoretically the index of refraction pattern in all the relevant cases. The full theoretical description involves the solution of the propagation problem with a time-dependent model for quasi-steady-state solitons [17, 18], an anisotropic model for the two-dimensional soliton nonlinearity [19], and a fully vector model for light. Here, we limit our report to the predictions in Fig.(4), which are the numerical evaluation of the tensorial electro-optic index of refraction pattern δn_{pq} ($p, q = 1, 2$, and $1 = x$, $2 = y$) for relevant situations, i.e., in the one soliton geometry for V_+ (first row) and V_- (second row), and for the two-soliton-separator geometry (third row), in the simplified scheme of assuming a given z-independent space-charge density ρ that corresponds to the steady-state solution for the observed soliton intensity, and calculating the electric field $\mathbf{E}$. Experiments can be understood on the basis of this calculation. For V_+, for $\theta_{in} = \theta_{out} = 0$, the pattern of Fig.(4a)

#84618 - $15.00 USD Received 28 Jun 2007; revised 31 Aug 2007; accepted 2 Sep 2007; published 12 Oct 2007
(C) 2007 OSA

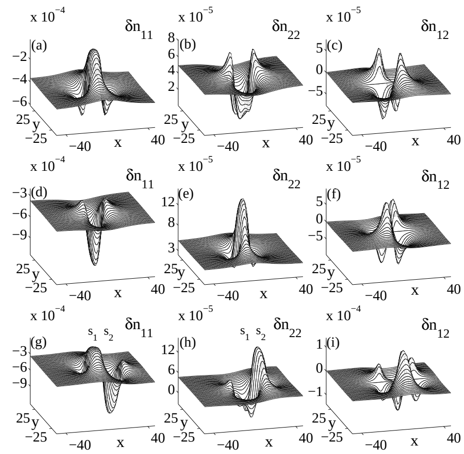

Fig. 4. Numerically evaluated components of the refractive index tensor driving light propagation through the readout stage: single channel readout for $V = V_{sol}$ (a,b and c), single channel readout for $V = -V_{sol}$ (d,e and f), two channels readout for $V = V_{S_1} = -V_{S_2}$ (g,h and i). Transverse x and y coordinate are expressed in microns.

applies, and the beam is guided as observed in Fig.(1c), whereas for $\theta_{in} = \theta_{out} = \pi/2$, it is weakly antiguided by the pattern in Fig.(4b), as observed in Fig.(1d). Coupling from one component to the other afforded by the δn_{12} (Fig.(4c)), generating a transmission for $\theta_{in} = 0$ and $\theta_{out} = \pi/2$ (and for $\theta_{in} = \pi/2$, $\theta_{out} = 0$), is reduced both because of the limited value of the pattern and because the effect is confined to regions external to the actual central waveguide core. For V_-, $\theta_{in} = \theta_{out} = 0$, the pattern of Fig.(4d) applies, and the beam is strongly anti-guided (as observed in Fig.(1g)), whereas for $\theta_{in} = \theta_{out} = \pi/2$, it weakly guided (Fig.(4e) and associated observation Fig.(1h)). Coupling from one component to the other afforded by the δn_{12} (Fig.(4f)), generating a transmission for $\theta_{in} = 0$ and $\theta_{out} = \pi/2$ (and for $\theta_{in} = \pi/2$, $\theta_{out} = 0$), is again reduced as observed. For the two-soliton polarization separator, for $V = V_{S_1} = V_{sol}$, for $\theta_{in} = 0$, the S_1 is guiding and S_2 is antiguiding (Fig.(4g)), whereas for $\theta_{in} = \pi/2$ S_2 is guiding and S_1 is antiguiding (Fig.(4h)), and the weak pattern in Fig.(4i) implies a weak polarization rotation, as observed. Since S_1 and S_2 are in close proximity, the $\theta_{in} = 0$ component of the input read-out beam is extracted from its original launch position and axis (i.e., along the S_2 pattern) into that of S_1 and *guided* by it as in Fig.(1c). In turn, the $\theta_{in} = \pi/2$ component remains trapped in the pattern of S_2, since it is guided by it as in Fig.(1h), explaining the results of Fig.(3d-f).

6. Conclusion

We have analyzed the propagation dynamics of a beam of arbitrary linear polarized light in electro-activated soliton patterns, and have identified a condition in which a two-soliton switching scheme serves to separate the input polarization components into two guided modes. This can be integrated with units already available, which are fiber-coupled waveguides, miniaturized electro-activated switches, hybrido-dimensional wavelength filters [20], permanent dielectric striation patterns and ion implantation structures, with the ultimate aim of demonstrating a versatile optical bench in a single solid state crystal of KLTN. Possible applications are in polarization encoding for innovative communications links such as single photon quantum cryptography schemes.

Research was funded by the Italian Ministry for Research through the FIRB initiative.

#84618 - $15.00 USD Received 28 Jun 2007; revised 31 Aug 2007; accepted 2 Sep 2007; published 12 Oct 2007
(C) 2007 OSA